South Pacific Eastern Subtropical Mode Water [*]

ANNIE P.S. WONG
Joint Institute for Marine and Atmospheric Research, University of Hawaii, and NOAA/Pacific Marine Environmental Laboratory, Seattle, Washington

GREGORY C. JOHNSON
NOAA/ Pacific Marine Environmental Laboratory, Seattle, Washington

[*] JIMAR manuscript 02-343. PMEL Contribution Number 2482.

Corresponding author address: Annie Wong, 7600 Sand Point Way, Bldg.3, Seattle, WA 98115-6349, USA. Email: awong@pmel.noaa.gov

ABSTRACT

We analyze the structure, formation, and destruction of South Pacific Eastern Subtropical Mode Water (SPESTMW). Geographic extent and water properties are discussed by using high quality CTD sections collected between 1991 and 1996. Defined as having a planetary potential vorticity magnitude of less than 3×10^{-10} $m^{-1}s^{-1}$, SPESMTW has a volume of about 1.1×10^{15} m^3, estimated from CTD data. The ventilation of this mode water is described by using data from a high-resolution XBT section in concert with 30-month time series from profiling CTD floats, some of the first Argo deployments. Published subduction rates allow a mode water formation rate estimate of 8.7×10^6 m^3 s^{-1}. Combining this estimate with the volume yields a residence time of about 4 years. The density-compensating covarying patterns of late winter surface temperature and salinity in the ventilation region of SPESTMW are shown to contribute to the strength of the mode water. However, while the destabilizing salinity gradient in SPESTMW contributes to its formation, it may also hasten its destruction by leaving it susceptible to double-diffusive convective mixing. SPESTMW spreads northwestward from its ventilation region within the subtropical gyre, eventually joining the South Equatorial Current. We speculate that the proximity of the SPESTMW ventilation region to the tropics, where winds and sea surface temperatures vary significantly, coupled with a direct interior circulation pathway to the equator, may allow SPESTMW to effect modulation of ENSO dynamics.

1. Introduction

In the eastern part of the subtropical gyres of the Pacific and the Atlantic oceans, a type of mode water exists in the vicinity of the seasonal and permanent pycnoclines. These mode waters (Type II in Hanawa and Talley (2001)) have been collectively termed eastern Subtropical Mode Water (STMW). They are located equatorward of the subtropical fronts and to the west of the coastal upwelling areas associated with the eastern boundary currents. In the North Atlantic, eastern STMW has been called Madeira Mode Water by Siedler et al. (1987) because of the closeness of its ventilation region to Madeira, an island located south of the Azores Front. In the South Atlantic, Provost et al. (1999) noted that mode waters in the east of the basin were probably ventilated by the Agulhas Current extensions or rings. In the North Pacific, Hautala and Roemmich (1998) identified eastern STMW as being associated with the water mass boundary between the eastern subtropical waters and the southward extension of subpolar waters along the California coast.

In the subtropical South Pacific, eastern STMW was recently described by Tsuchiya and Talley (1996) as a thick layer of subtropical water above the halocline, using data from the World Ocean Circulation Experiment (WOCE) hydrographic section P17 at 135° W. It was subsequently observed as a pycnostad along other WOCE sections in the eastern South Pacific, and was hypothesized to be a remnant of the winter mixed layer in the eastern South Pacific equatorward of the subtropical front, where high surface salinities may be responsible for creating thick winter mixed layers (Tsuchiya and Talley 1998). The 'subtropical front' referred to here is the band along the poleward edge of the subtropical gyres in the southern hemisphere, where surface salinity decreases poleward rapidly to 34.5 (Tomczak and Godfrey (1994), Stramma et al. (1995)). It is found south of 30° S, is almost circumpolar in extent (disrupted only by the land masses of South America and New Zealand), and is often used to delimit the northern geographic extent of the Southern Ocean.

From hereon we will use the name South Pacific Eastern Subtropical Mode Water (SPESTMW), after Hanawa and Talley (2001). Of all the eastern STMWs of the world ocean, SPESTMW occupies the largest lateral area (see Plate 5.4.3 in Hanawa and Talley (2001)). Detailed study of SPESTMW is possible using a variety of recently available data sources, including autonomous conductivity-temperature-depth (CTD) profiling floats deployed in the southeastern tropical Pacific in 2000 as part of the Argo program. The purposes of this paper are to describe the water properties, geographic extent, and circulation of SPESTMW, as well as to explore its formation and destruction mechanisms. We show that SPESTMW is a persistent and distinct water mass, that part of it is ventilated at relatively low latitudes, and that its prominence, formation, and destruction are all closely tied to the salinity distribution of the eastern subtropical South Pacific. The various data sets employed in this study are described in the sections where they are introduced.

2. Spatial Extent and Water Properties of SPESTMW

Synoptic CTD sections provide accurate measurements of temperature and salinity with high spatial resolution. Hence we begin the description of SPESTMW by examining high quality CTD sections in the South Pacific (Fig. 1). We have chosen five meridional sections east of the dateline, and two zonal sections nominally at 17° S and 32° S. These sections were all collected as part of the World Ocean Circulation Experiment (WOCE), between 1991 and 1996, and are available from the WOCE Hydrographic Program Office website (http://whpo.ucsd.edu). These sections were all accompanied by in-situ bottle measurements for calibration, and are thought to be accurate to 0.002° C in temperature, 0.003 in salinity, and 0.1% in pressure. All potential density anomaly values in this paper are referenced to zero pressure (σ_θ).

FIG. 1.

We choose planetary potential vorticity (Q) as the primary identifier of SPESTMW because Q is a conservative quantity, which is only altered by mixing processes and

surface forcing. Here $Q = (f/g)N^2$, where $N^2 = -(g/\rho)(d\rho/dz)$ is the buoyancy frequency squared, a measure of the vertical stratification, f is the Coriolis parameter, g is the acceleration of gravity, and ρ is the density locally referenced to the central value of adjacent observed pressure levels, between which its vertical gradient is estimated. We smooth Q vertically with a 26-dbar half-width Hanning filter, appropriate to the vertical scale of the pycnocline. Note that while Q is negative in the southern hemisphere, we refer only to its absolute value $|Q|$ hereafter.

The SPESTMW pycnostad described by Tsuchiya and Talley (1998) along the WOCE P19 section at 88° W has $|Q| < 3 \times 10^{-10}$ m^{-1} s^{-1}. We select this value to define the $|Q|$ minimum layer associated with SPESTMW. Note that there are other areas in the vertical sections that have $|Q|$ values below this threshold. One of these is in the surface mixed layer above the pycnocline where stratification is absent. Another is in the deep ocean well below the pycnocline where N^2 is very low. A third is near the equator where f vanishes. However, except in its ventilation region in the late winter, where it is in direct contact with the atmosphere through the mixed layer, the $|Q|$ minimum layer of SPESTMW can be seen as a distinct body separate from other low stratification and equatorial areas. The only other feature that might be confused with the SPESTMW $|Q|$ minimum is the Pacific Equatorial 13° C Water, that has been argued to be ventilated near Tasmania (Tsuchiya 1981). This water mass forms a distinct pycnostad between 100 and 400 dbar below the Equatorial Undercurrent, and is flanked on either side by the subsurface countercurrents (Johnson and Moore 1997). However, with σ_θ greater than 26.0 kg m^{-3}, it is denser than SPESTMW, as well as geographically separated.

a. Spatial Extent of SPESTMW

Along the three easternmost meridional WOCE sections at 88° W (P19), 103° W (P18) and 135° W (P17), SPESTMW is clearly seen as a distinct $|Q|$ minimum

layer (Figs. 2 - 4). SPESTMW is present as a well-developed thermostad, halostad, and pycnostad (hence $|Q|$ minimum) along 88° W and 103° W. It extends from the subtropical front at 33° S equatorward to 14° S, along 88° W. Along 103° W, it occupies a similar latitude span, from 32° S to 10° S, but is shifted slightly equatorward. At higher latitudes along 88° W and 103° W, SPESTMW is found between the seasonal and permanent thermoclines, while at lower latitudes, it is embedded within the permanent thermocline. The SPESTMW $|Q|$ minimum is weaker along 135° W compared with the two sections to the east, but is still well-defined and here embedded entirely within the permanent thermocline. At this longitude, the $|Q|$ minimum is located further equatorward, between 23° S and 7° S.

Further to the west (not shown), the $|Q|$ minimum layer of SPESTMW begins to diminish. It can still be seen between 16° S and 5° S along 150° W (P16), but by 170° W (P15), a coherent $|Q|$ minimum layer is no longer evident. On the other hand, the western STMW becomes evident on somewhat denser surfaces south of 25° S along 170° W. SPESTMW therefore is a distinct water mass separate from the western STMW north of New Zealand described by Roemmich and Cornuelle (1992). This clear separation between eastern and western STMWs has been observed in the North Atlantic by Siedler et al. (1987), and in the North Pacific by Hautala and Roemmich (1998). It is this east-west distinction that prompted previous investigators to look towards the eastern basins for a separate ventilation region, away from the more traditional subtropical mode water ventilation areas associated with the western boundary currents.

The spatial extent of SPESTMW observed along the two zonal WOCE sections (not shown) at 32° S (P6) and 17° S (P21) are consistent with those observed along the meridional sections. Along the southernmost section at 32° S, the $|Q|$ minimum layer of SPESTMW is evident between 115° W and 85° W, while the western STMW can be seen west of 140° W. Along 17° S, the $|Q|$ minimum of SPESTMW can be traced as far west

as 145° W, and as far east as 83° W. The western STMW cannot be seen along 17° S.

The spatial extent of SPESTMW as indicated by these WOCE sections is oriented roughly along a WNW-ESE axis (Fig. 1). Some of it eventually moves westward and equatorward in the South Equatorial Current (Johnson and McPhaden 1999). The depths at which SPESTMW is found change as the $|Q|$ minimum layer rises and dives following the subtropical gyre. At its southern extent near the subtropical front, SPESTMW can be found at about 150 dbar. It shoals equatorward with the pycnocline, so that at around 10° S and east of 100° W, SPESTMW is found as shallow as 80 dbar. Further to the west, it dives with the pycnocline toward the center of the subtropical gyre, so that at around 20° S and west of 100° W, SPESTMW can be found as deep as 200-300 dbar. The furthest we can trace the $|Q|$ minimum layer is to 10° S, 150° W. There, SPESMTW is found at about 200 dbar.

b. Water Properties of SPESTMW

SPESTMW displays a wide range of temperature values. While SPESTMW is a prominent thermostad, the weak vertical temperature gradient is still stabilizing (decreasing with increasing pressure) within the $|Q|$ minimum layer. In the horizontal, SPESTMW is colder to the southeast and warmer to the northwest, reflecting the late winter surface temperature distribution of the southeast Pacific (Antonov et al. 1998). Along WOCE P19, the easternmost section at 88° W, potential temperature θ of SPESTMW rises from 13.3-15.5° C at its southernmost extent near 33° S, to 18-19° C at its northern limit near 14° S (Fig. 2 a). Temperature is higher to the west along 103° W, where θ ranges from 16-18° C at 33° S, to 19-23° C at 10° S (Fig. 2 b). Along 135° W, temperatures within the $|Q|$ minimum layer range from 17-19° C at 23° S to 18-22° C at 7° S (Fig. 2 c). The full temperature range along 135° W is slightly less than that along 103° W, consistent with some mixing and destruction of SPESTMW along its advection path after subduction. Note that the mixed layer along P17 is deeper than P18 and

P19, as P17 was sampled during the austral winter. FIG. 2.

SPESTMW also displays a wide range of salinity values. However, in contrast to temperature, the vertical salinity distribution is destabilizing (decreasing with increasing pressure). The horizontal salinity distribution within SPESTMW is fresher in the southeast and saltier in the northwest, reflecting the mean surface salinity distribution of the southeast Pacific (Boyer et al. 1998). Salinity increases from a low of 34.3 at the southern limit along 88° W, to 35.5 at the northern limit (Fig. 3 a). Salinities are higher along 103° W, ranging from 34.8 to 36.2 from south to north (Fig. 3 b). Along 135° W, salinities range from 35.2 to 36.2 (Fig. 3 c). Again, the slightly smaller range of salinity along 135° W suggests that by this longitude, SPESTMW is isolated from surface forcing, and is being slowly destroyed by mixing as it is advected northwestward. FIG. 3.

The coldest ($\theta < 15.5°$ C), freshest (S < 34.6), and densest ($\sigma_\theta > 25.53$ kg m^{-3}) SPESTMW is found towards the southeast, east of 90° W and south of 32° S. The densest SPESTMW observed in all the WOCE sections has $\sigma_\theta = 25.74$ kg m^{-3}, at the southern end of WOCE P19 (Fig. 4 a). In general, SPESTMW occupies the σ_θ range of 25.0-25.7 kg m^{-3}. FIG. 4.

Despite the wide range of temperature and salinity values, SPESTMW occupies a relatively small density range because its temperature and salinity distributions covary in a density-compensating sense (Fig. 5). In other words, in the vertical, warm salty water overlies cold fresh water. In the horizontal, wintertime surface water properties range from colder and fresher in the southeast to warmer and saltier in the northwest. Thus, the (lateral and vertical) density range of SPESTMW is only about 0.4 of that which would be indicated by the temperature range alone, assuming a constant mid-range salinity value. While the vertical salinity distribution does not dominate over temperature to destabilize the water mass, it does significantly reduce its stratification in the vertical. Likewise, the regional surface salinity distribution allows ventilation of a relatively constant density over a large surface area. FIG. 5.

3. Formation and Destruction of SPESTMW

The wide range of temperatures and salinities in SPESTMW suggests that it is ventilated over a large area. To study formation of SPESTMW in the context of the seasonal cycle, we introduce data from autonomous CTD profiling floats (Fig. 1). To directly illustrate wintertime ventilation, we use expendable bathythermograph (XBT) data (Fig. 1). We also estimate a SPESTMW formation rate by combining information from the monthly climatologies of the World Ocean Atlas 1998 (Antonov et al. (1998), Boyer et al. (1998)) with subduction rate estimates of Huang and Qiu (1998). We corroborate this formation rate with a geostrophic transport estimate by using the WOCE data downstream of the ventilation region. We then use the formation rate and the volume estimate to gain a crude measure of SPESTMW residence time. Finally, expanding on the findings of Tsuchiya and Talley (1998), we use the WOCE data to argue for the importance of double-diffusive mixing in the destruction of SPESTMW.

a. Data

In July 2000, the U.S. Argo program began its first deployments of autonomous CTD profiling floats in the eastern South Pacific. By January 2003, ten active Argo floats sampling in the area downstream of the SPESTMW ventilation region have accumulated up to 30 months of data, with each of these floats sampling as many as three austral winters. These floats park at a predetermined subsurface pressure for a period of around 10 days, then collect CTD data at roughly 50-70 discrete pressures from a mid-depth profiling pressure to near the surface. The floats then remain on the surface for about a day to determine their surface drift and to transmit the data via satellite, before sinking to the parking pressure and beginning the cycle anew. Some float salinities are often quite stable for long periods, but others drift more rapidly. We have corrected sensor-related drifts in float salinity values using climatological data from areas of the water column exhibiting low variability (Wong et al. 2003). Potential

densities and potential vorticities have been calculated from these corrected salinities.

In addition to these profiling floats, data are also available along a high resolution (HRX) expendable bathythermograph (XBT) line, PX81, from Honolulu to Chile (http://www.hrx.ucsd.edu). On HRX lines, XBTs are dropped every 30-40 km along the ship track to obtain temperature-depth profiles, supplemented by salinity data from much more infrequent expendable CTD (XCTD) drops. Sampling of PX81 began in 1997 and is ongoing at a rate of four cruises a year. Salinities estimated along this XBT line are based on a blend of the sparse XCTD data and a salinity climatology, as detailed in Gilson et al. (1998). Potential density and $|Q|$ have been calculated using the estimated salinities.

b. Seasonal Cycle of Mixed Layer

All of the ten profiling floats (Fig. 1) are sampling in an area where the winter mixed layer is lighter than 25.0 kg m^{-3}. In other words, the winter mixed layer there is not dense enough to ventilate SPESTMW. However, the CTD data from these floats have enabled us to observe the seasonal evolution, over nearly three annual cycles, of the mixed layer structure in the South Pacific, where previously only climatological and synoptic data are available.

The time series from float 10 (WMO ID 59019), the southernmost of these floats, is classic. The seasonal cycle of mixed-layer depth, near-surface potential temperature, and near-surface potential density for float 10 follows a saw-tooth like pattern (Fig. 6). The mixed layer temperature is highest during the austral summer, between January and March. From February onwards, the mixed layer gradually deepens. Initial deepening is presumably caused by wind-driven mixing, since the near-surface density (temperature) is still generally decreasing (increasing) even as the mixed layer deepens. However, from April onwards, convective processes dominate until the late austral winter or early spring, as the surface temperature drops and the mixed layer eventually deepens to

about 150 dbar, eating into the seasonal thermocline. By November, as the surface temperature rises, the deep winter mixed layer is very quickly capped by a shallow seasonal thermocline. The seasonal thermocline strengthens as the surface temperatures increase into the austral summer, when the cycle beings anew.

FIG. 6.

The mixed layer is deepest during October. It starts to retreat by the end of October, and reaches its shallowest depth by the beginning of December. Thus the retreat of the winter mixed layer, as indicated by the time difference between when the mixed layer depth goes from deepest to shallowest (Fig 6 a), happens over 1 month (November) in this part of the subtropical gyre. This rapid retreat of the winter mixed layer is a condition for the 'Stommel demon' selection (Stommel 1979), where mixed layer fluid with late winter properties is subducted into the permanent thermocline (Huang and Qiu 1998).

Interestingly, there is no obvious seasonal cycle to the near-surface salinity (Fig. 6 d) in this float (or any of the others). The slowly varying near-surface salinity has about 1/4 of the effect on density compared with that of the seasonally varying near-surface temperature. Thus, initial Argo data suggest that in a one-dimensional sense, there is not a large role of seasonal salinity variations in wintertime convective mixing and SPESTMW formation.

Float 10 drifted in the area 119°-124° W, 18°-21° S. Between June and October, the mixed layer (as indicated by low $|Q|$ in Fig. 7 c) can be seen to ventilate to σ_θ slightly lighter than 25.0 kg m^{-3}. Float 9 (WMO ID 39031), to the northeast of float 10, displays a similar pattern. Further south of these latitudes, the winter mixed layer density is sufficiently high to directly ventilate SPESTMW (Antonov et al. (1998), Boyer et al. (1998)). This cycle will be fully illustrated when the Argo array is extended to the south of its present range. The band of low $|Q|$ where $25.0 < \sigma_\theta < 25.7$ kg m^{-3} (Fig. 7 c) is SPESTMW observed along this float's drift track. At this location, SPESTMW is found between 150 and 300 dbar, and is embedded within the permanent pycnocline.

Its continuous presence in this time series indicates that here, SPESTMW is a water mass that is present throughout the year. FIG. 7.

A time series further downstream of the ventilation region, from float 5 (WMO ID 59016), contrasts sharply with the previous data (Fig. 8). As with float 10, this time series started in July 2000 during the austral winter. Being further to the west and closer to the equator, winter mixed layer salinity for float 5 is fresher than that for float 10, and surface temperatures are generally warmer. The winter mixed layer reaches down to only about 80 dbar, and with σ_θ lighter than 23.8 kg m^{-3}, much lighter than SPESTMW. The winter mixed layer here retreats more gradually, as opposed to the rapid retreat seen in float 10. A subsurface salinity maximum is present between 100 and 150 dbar as a year-round feature. Thus the local near-surface salinity gradient is stabilizing. This subsurface salinity maximum has been referred to as 'Subtropical Water', 'Tropical Water', and more recently as 'Subtropical Underwater' (STUW) by O'Connor et al. (2002), who estimated its formation rate at 6-7 Sv. At this location (124°-133° W, 8°-12° S), SPESTMW persists as a year-round thin layer centered at around 150 dbar. It sits below STUW, which acts as a block that prevents any local surface forcing from reaching SPESTMW. FIG. 8.

c. Ventilation Region of SPESTMW

While the profiling floats presently deployed in the South Pacific are not quite far enough south to show direct SPESTMW wintertime ventilation, the HRX section P81 does cross the ventilation region. Here we discuss the section from Aug-Sep 1998 (Fig. 1), because it was occupied during late austral winter, at the end of the seasonal mode water ventilation period, when mixed layer density and depth are at their maxima.

Along the ship track of the Aug-Sep 1998 PX81 section (Fig. 1), the $|Q|$ minimum layer of SPESTMW extends from the subtropical front at about 33° S, equatorward to about 8° S (Fig. 9). Surface density at the subtropical front reaches 25.7 kg m^{-3} in

September, which approaches the highest density of SPESTMW observed along the WOCE sections. The lightest density surface of SPESTMW, 25.0 kg m^{-3}, outcrops at about 22° S along the Aug-Sep 1998 PX81 track (Fig. 9 c), near the southern edge of the core of highly saline water centered at 20° S (S > 36.4, Fig. 9 b, near 125° W along the 1998 XBT line). The winter mixed layer reaches a depth of about 200 dbar between the subtropical front and 20° S, sufficiently dense to ventilate and replenish the SPESTMW density range.

FIG. 9.

The very saline surface water (S > 36.2) between 15 and 25° S along PX81, which can also be seen along the WOCE sections of P17, P18, P21 (Fig. 3), and float 10 (Fig. 7), is due to the climatology of the eastern subtropical South Pacific, where annual mean evaporation greatly exceeds precipitation (Oberhuber 1988). This saline surface water extends equatorward after subduction as STUW. There, SPESTMW rides underneath STUW, as seen in the time series of float 5 (Fig. 8). At these lower latitudes, surface temperatures increase equatorward while surface salinities decrease, both of which are stabilizing. Thus, north of the core of saline surface water, SPESTMW is isolated from any surface forcings by the warm, fresh, light surface water. Hence it is not surprising that the $\sigma_\theta = 25.0$ kg m^{-3} outcrop line (the lightest isopycnal of SPESTMW) is in the proximity of the axis of the core of saline surface water.

The ventilation region of SPESTMW therefore is an area in the eastern South Pacific bounded roughly by the subtropical front to the south, the axis of the core of saline surface water to the northwest, and the offshore edge of the upwelling area along the Chilean coast. The subtropical gyre advects water northwestward in this area. During its transit across the ventilation region, the SPESTMW thickness increases due to direct contact with atmospheric forcing, so $|Q|$ within SPESTMW is not conserved in this area. The thickest SPESTMW layer therefore is found just downstream of the edge of the ventilation region, in the vicinity of 20° S, 110° W.

South of the subtropical front, surface salinity reaches a meridional minimum of

less than 34.4. This fresh surface salinity, which can be seen at the southern end of WOCE P18 (Fig. 3 b) and P19 (Tsuchiya and Talley 1998), and the eastern end of P6 (Wijffels et al. 2001), is responsible for the formation of the shallow salinity minimum of the South Pacific (Reid 1973). The presence of this cold, fresh surface water to the southeast, and the core of warm, saline surface water north of 20° S, means that both surface temperature and salinity decrease towards the southeast in the SPESTMW ventilation region (Antonov et al. (1998), Boyer et al. (1998)). As discussed previously, these mean surface water property distributions are density-compensating. Hence while the range of surface temperature and salinity is large over the ventilation region, the surface density range is relatively small. It is because surface water with such a narrow density range exists over such a wide subduction area, that allows the formation of a large volume of this mode water. The fact that SPESTMW is cooler and fresher to the southeast, and warmer and saltier towards the northwest, means that SPESTMW is largely reflecting the gyre properties where it is ventilated. Thus, although seasonal variation in mixed layer salinity is not a significant factor in SPESTMW formation, as discussed previously, the mean geographic distribution of surface salinity certainly has an impact on the formation of SPESTMW.

d. Formation

We have identified the area in the eastern South Pacific where wintertime convective mixing is strong enough to replenish SPESTMW. Float data from the vicinity of the ventilation region have demonstrated that the seasonal cycling of the mixed layer there is conducive to subduction of late winter mixed layer properties. The actual formation of SPESTMW then requires subduction of this water into the permanent thermocline. Here, we estimate the annual mean formation rate of SPESTMW by using the South Pacific subduction rates of Huang and Qiu (1998). In their study of the circulation of the subtropical South Pacific, Huang and Qiu (1998) calculated the annual mean

subduction from a diagnostic model based on Stommel (1979). Subduction due to both Ekman pumping and lateral induction has been calculated in Lagrangian coordinates, with isopycnal velocity (assuming a level of no motion at 2000 m) and Ekman pumping velocity estimated from climatological data.

The ventilation region of SPESTMW can be roughly defined by where the maximum surface σ_θ from the World Ocean Atlas 1998 monthly climatology (Boyer et al. (1998), Antonov et al. (1998)) lies between 25.0 and 25.7 kg m^{-3}. Summing the areas where the subduction rate is positive (negative is 'obduction', where water from the thermocline flows into the mixed layer) east of 140° W and between the bounding maximum surface potential isopycnals of 25.0 and 25.7 kg m^{-3} (Fig. 10) gives a SPESTMW formation rate estimate of about 8.7×10^6 m^3 s^{-1}.

FIG. 10.

To corroborate this formation rate estimate, a second indirect estimate is made by examining geostrophic transport of this water mass downstream of its ventilation region. WOCE sections P17 (135° W) and P21 (17° S) are located to the west and north of the SPESTMW ventilation region, respectively (Figs. 1 and 10), and intersect near 133° W, 17° S. By joining the portion of P17 located south of this intersection with the portion of P21 east of the same, we can calculate the net geostrophic transport of SPESTMW downstream of its ventilation region. We reference the geostrophic velocities to 2000 dbar (following Huang and Qiu (1998)), and estimate the net transport in the $|Q|$ minimum layer. The resulting transport estimate is 7.2×10^6 m^3 s^{-1} to the north and west, which is similar to but smaller than the formation rate estimate above. This difference is to be expected since the transport estimate is made somewhat downstream of the ventilation region. Both estimates are relatively insensitive to the reference level, so long as it remains below the pycnocline and above the influence of the bottom boundary layer, since deep geostrophic shear is weak in these sections compared with that in the pycnocline (where SPESTMW is embedded).

We then use the WOCE sections to make a rough estimate of the SPESTMW

volume. The depth interval for each station over which $|Q| < 3 \times 10^{-10}$ m^{-1} s^{-1} and $25.0 < \sigma_\theta < 25.7$ kg m^{-3} is determined for each WOCE section. The areal distribution of these SPESTMW thicknesses is then interpolated by objective analysis onto a $2^\circ \times 2^\circ$ grid. By integrating these interpolated thicknesses over the area occupied by SPESTMW, we estimate that SPESTMW has a volume of about 1.1×10^{15} m^3. The uncertainty of this volume estimate is about 10%, due mainly to the error from the interpolation.

Dividing the volume by the formation rate of 8.7×10^6 m^3 s^{-1} gives a residence time of about 4 years for SPESTMW. This time scale is comparable to apparent ages based on the partial pressure of CFC-11, which range from 0 to 15 years on $\sigma_\theta = 25.4$ kg m^{-3} within the area encompassing SPESTMW (J. Bullister, personal communication 2002).

e. Destruction

SPESTMW is eroded by diffusion as it is advected northwestward in the South Equatorial Current, and eventually can no longer be identified as defined by our low $|Q|$ criterion. Here we demonstrate the strong potential for salt fingering in SPESTMW, that likely hastens the erosion of this mode water. This propensity has already been shown in the east using WOCE P19 data (Tsuchiya and Talley 1998). Here we expand similar calculations to the west and over several annual cycles.

The stability ratio, $R_\rho = (\alpha/\beta)(T_z/S_z)$, quantifies susceptibility to salt fingering (Schmitt 1981). Here α is the thermal expansion coefficient, β is the haline contraction coefficient, T_z is the vertical temperature gradient, and S_z is the vertical salinity gradient. In regions where the vertical salinity gradient is sufficiently destabilizing that values of R_ρ dip below 2 and approach 1, salt fingering, a double diffusive type of convective mixing, becomes increasingly vigorous (Schmitt 1981).

As previously discussed, a strong destabilizing vertical salinity gradient arises in SPESTMW from the contrast between the subsurface salinity maximum lying above

and to the northwest of the SPESTMW ventilation region, and the shallow salinity minimum which lies below and to the southeast. Whether this gradient is likely to promote elevated mixing by salt fingering can be diagnosed by computing R_ρ from WOCE and profiling float CTD data.

The meridional WOCE sections P17-P19 illustrate the spatial pattern of R_ρ (Fig. 11). Near the eastern edge of the ventilation region, along P19 at 88° W, values of R_ρ are well below 2 along most of the base of SPESTMW. They even reach below 1.5 in a few isolated locations, suggesting the presence of very strong salt fingering (Schmitt 1981). Along P18 at 103° W, near the center of the ventilation region, nearly all of SPESTMW except its uppermost reaches has values of R_ρ below 2, again with some areas below 1.6.

To the west of the ventilation region, along P17 at 135° W, the $|Q|$ signature of SPESTMW has been eroded significantly. Coincident with this erosion, there is only a small isolated area in the center of the remaining SPESTMW where $1.9 < R_\rho < 2$ can be seen (Fig. 11), indicating potential for salt fingering, but neither as vigorous nor as widespread as to the east. Therefore it appears that salt fingering is strong at the base of SPESTMW within the ventilation region, and continues somewhat downstream, but eventually diminishes, after significantly eroding the mode water itself. FIG. 11.

This is confirmed by the float array, where only floats 9 (WMO ID 39031) and 10 show R_ρ values below 2 in the SPESMTW range. In addition, their time series (Fig. 12) suggest that just as SPESTMW persists all year long, so does the potential for salt fingering. FIG. 12.

As discussed above, the salinity distribution plays a two-fold role in strengthening SPESTMW by first reducing the lateral density gradient in the ventilation region and then reducing the vertical density gradient in the subducted water. Ironically, this same vertical salinity gradient likely hastens SPESTMW destruction by enabling strong mixing processes that erode it.

4. Summary and Discussions

SPESTMW is a water mass that persists all year long, and is geographically distinct from the western STMW found north of New Zealand. Near its origin, SPESTMW is present as a thermostad, a halostad and a pycnostad. After formation, it is carried along by the eastern limb of the South Pacific subtropical gyre, northwestward towards the equator underneath the salinity maximum of STUW, and eventually joins the South Equatorial Current. It is traceable as a layer with $|Q| < 3 \times 10^{-10}$ m^{-1} s^{-1}. The furthest we can trace it by this $|Q|$ criterion is to about 150° W, 10° S.

SPESTMW exhibits a wide range of temperature and salinity characteristics that resembles the surface water properties distribution in the eastern subtropical South Pacific, indicating that it is ventilated over a wide area, and that it retains the memory of the subtropical gyre as it is formed. Examination of winter mixed layer densities along a PX81 XCTD/XBT line and along the drift tracks of profiling floats shows that winter convective mixing in the eastern South Pacific is strong enough to replenish SPESTMW. Its ventilation region has been identified to be the area south of the core of saline surface water, north of the subtropical front, and west of the coastal upwelling area along South America. Combining a volume estimate of 1.1×10^{15} m^3 and a formation rate estimate of 8.7×10^6 m^3 s^{-1}, we estimate that SPESTMW has a residence time of about 4 years.

In the eastern South Pacific, initial Argo data demonstrate that seasonal salinity variation is not a big factor governing the strength of wintertime convective mixing, and therefore winter mixed layer depths. However, the spatial salinity distribution does enable the formation of a large volume of mode water. While the temperature and salinity characteristics within SPESTMW have a wide range, they covary in a density-compensating manner so that warm waters are salty and cold waters are fresh. This pattern reduces the wintertime surface density gradient over a wide region, contributing to the strength and extent of SPESTMW. The density-compensating surface salinity gradient becomes a destabilizing vertical salinity gradient after subduction, further

strengthening the low $|Q|$ signature of SPESTMW. However, this vertical gradient also hastens SPESTMW destruction by leaving it susceptible to double diffusion.

In the eastern North Pacific, Hosoda et al. (2001) demonstrated that the weak gradients in surface temperature and salinity resulted in wide spacing between outcrop lines, which was most important for the low $|Q|$ formation of the eastern STMW there. Ladd and Thompson (2001) also concluded that the thickness maxima in the eastern STMW layers of the North Pacific were the result of wide layer outcrop, which was at least partially due to weak summer heating (Ladd and Thompson 2000). Wide spacing between outcrop lines therefore seems to be the common basis for the existence of these volumetric modes in the eastern North and South Pacific. This formation condition is very different from that of the traditional STMWs associated with the western boundary currents (Type I in Hanawa and Talley (2001)), whose formation is due to intense wintertime cooling.

Float data from the vicinity of the SPESTMW ventilation region show that the winter mixed layer there retreats rapidly (in 1 month). Such large amplitude seasonal cycling is necessary for the 'Stommel demon' subduction process to take place. This favourable mixed layer condition, coupled with abundant spatial features in surface property distribution, make the eastern South Pacific rich in water mass formation. Lying at depths below SPESTMW, at density about 26.0 kg m^{-3} and with salinity about 34.4 is the shallow salinity minimum of the South Pacific (Reid 1973). At even higher densities are Subantarctic Mode Water and Antarctic Intermediate Water (McCartney 1982). These water masses are all formed in the eastern South Pacific and all spread similarly northwestward in the subtropical gyre, eventually heading towards the equator in the South Equatorial Current. The eastern South Pacific is therefore a major formation area for water masses that ventilate the shallow and intermediate layers of the subtropical gyre, which makes this a climatically-sensitive region.

Some of the SPESTMW ventilation region actually lies within the tropics (Fig. 10).

Even the edge of the tropics shows considerable variability in sea surface temperature and surface winds on interannual ENSO time scales and and on decadal time scales associated with the Pacific Decadal Oscillation (Zhang et al. (1997), Mantua et al. (1997), Harrison and Larkin (1998)). Hence there is potential for variations in water properties and subduction rates of SPESTMW on interannual time-scales. Since at least some SPESTMW follows a relatively rapid, direct interior pathway to the equator (Johnson and McPhaden 1999), variability in its formation rate or water properties could influence El Nino variability on decadal time scales (Kleeman et al. (1999), Gu and Philander (1997), Giese et al. (2002)).

Only data collected over the past decade has allowed this study to be undertaken. The quasi-synoptic WOCE CTD and HRX sections with their high spatial resolution but sparse temporal coverage are nicely complemented by the Argo floats with their high temporal resolution but as yet limited spatial coverage. The hypothesis that there is significant interannual variability in the characteristics or formation rates of SPESTMW will be more easily tested after the Argo array has been expanded to cover the SPESTMW ventilation region. The full Argo array, analyzed in concert with data from satellite altimeters and scatterometers, should be most illuminating.

Acknowledgments. We would like to thank Steve Riser, Dean Roemmich, Russ Davis, and John Gilson for the eastern South Pacific US Argo floats and data along the high resolution XBT/XCTD line of PX81. Bo Qiu generously provided comments and the subduction rate estimates from the study of Huang and Qiu (1998). Comments from two anonymous reviewers, as well as from Toshio Suga and John Toole, helped to improve the manuscript. Kristy McTaggart is acknowledged for her assistance with data processing. Lastly, we are much obliged to the many people who contributed to the WOCE Hydrographic Program in the South Pacific. This is a publication of the University of Hawaii pursuant to National Oceanic and Atmospheric Administration Award No. NA17RJ1230.

REFERENCES

Antonov, J., S. Levitus, T. Boyer, M. Conkright, T. O'Brien, and C. Stephens, 1998: *World Ocean Atlas 1998, Vol. 2: Temperature of the Pacific Ocean, NOAA Atlas NESDIS 28, 166 pp.*. U.S. Gov. Printing Office.

Boyer, T., S. Levitus, J. Antonov, M. Conkright, T. O'Brien, and C. Stephens, 1998: *World Ocean Atlas 1998, Vol. 5: Salinity of the Pacific Ocean, NOAA Atlas NESDIS 31, 166 pp.*. U.S. Gov. Printing Office.

Giese, B., S. Urizar, and N. Fučkar, 2002: Southern hemisphere origins of the 1976 climate shift. *Geophysical Research Letters*, **29**(2), 10.1029/2001GL013,268.

Gilson, J., D. Roemmich, and B. Cornuelle, 1998: Relationship of TOPEX/Poseidon altimetric height to steric height and circulation in the North Pacific. *Journal of Geophysical Research*, **103**(C12), 27,947–27,965.

Gu, D., and G. Philander, 1997: Interdecadal climate fluctuations that depend on exchanges between the tropics and extratropics. *Science*, **275**, 805–807.

Hanawa, K., and L. Talley, 2001: Mode waters. *Ocean Circulation and Climate - Observing and Modelling the Global Ocean*, G. Siedler, J. Church, and J. Gould, Eds., Academic Press, pp. 373–386.

Harrison, D., and N. Larkin, 1998: El Nino-Southern Oscillation sea surface temperature and wind anomalies, 1946-1993. *Reviews of Geophysics*, **36**, 353–398.

Hautala, S., and D. Roemmich, 1998: Subtropical mode water in the Northeast Pacific Basin. *Journal of Geophysical Research*, **103**(C6), 13,055–13,066.

Hosoda, S., S. Xie, K. Takeuchi, and M. Nonaka, 2001: Eastern North Pacific Subtropical Mode Water in a general circulation model: formation mechanism and salinity effects. *Journal of Geophysical Research*, **106**(C9), 19,671–19,681.

Huang, R., and B. Qiu, 1998: The structure of the wind-driven circulation in the subtropical South Pacific Ocean. *Journal of Physical Oceanography*, **28**, 1173–1186.

Johnson, G., and M. McPhaden, 1999: Interior pycnocline flow from the subtropical to the equatorial Pacific Ocean. *Journal of Physical Oceanography*, **29**, 3073–3089.

Johnson, G., and D. Moore, 1997: The Pacific subsurface countercurrents and an inertial model. *Journal of Physical Oceanography*, **27**, 2448–2459.

Kleeman, R., J. McCreary Jr., and B. Klinger, 1999: A mechanism for the decadal variation of ENSO. *Geophysical Research Letters*, **26**, 1743–1746.

Ladd, C., and L. Thompson, 2000: Formation mechanisms for North Pacific Central and Eastern Subtropical Mode Waters. *Journal of Physical Oceanography*, **30**, 868–877.

Ladd, C., and L. Thompson, 2001: Water mass formation in an isopycnal model of the North Pacific. *Journal of Physical Oceanography*, **31**, 1517–1537.

Mantua, N., S. Hare, Y. Zhang, J. Wallace, and R. Francis, 1997: A Pacific interdecadal climate oscillation with impacts on salmon production. *Bulletin of the American Meteorological Society*, **78**(6), 1069–1079.

McCartney, M., 1982: The subtropical recirculation of mode waters. *Journal of Marine Research*, **40, suppl.**, 427–464.

Oberhuber, J., 1988: *An atlas based on the COADS data set: the budget of heat, buoyancy and turbulent kinetic energy at the surface of the global ocean*. Max-Planck-Institut für Meteorologie.

O'Connor, B., R. Fine, K. Maillet, and D. Olson, 2002: Formation rates of subtropical underwater in the Pacific Ocean. *Deep-Sea Research*, **49**, 1571–1590.

Provost, C., C. Escoffier, K. Maamaatuaiahutapu, A. Kartavtseff, and V. Garçon, 1999: Subtropical mode waters in the South Atlantic Ocean. *Journal of Geophysical Research*, **104**(C9), 21,033–21,049.

Reid, J., 1973: The shallow salinity minima of the Pacific Ocean. *Deep-Sea Research*, **20**, 51–68.

Roemmich, D., and B. Cornuelle, 1992: The subtropical mode waters of the South Pacific Ocean. *Journal of Physical Oceanography*, **22**, 1178–1187.

Schmitt, R., 1981: Form of the temperature-salinity relationship in the Central Water: evidence for double-diffusive mixing. *Journal of Physical Oceanography*, **11**(7), 1015–1026.

Siedler, G., A. Kuhl, and W. Zenk, 1987: The Madeira Mode Water. *Journal of Physical Oceanography*, **17**, 1561–1570.

Stommel, H., 1979: Determination of water mass properties of water pumped down from the Ekman layer to the geostrphic flow below. *Proc. Natl. Acad. Sci., USA.*, **76**, 3051–3055.

Stramma, L., R. Peterson, and M. Tomczak, 1995: The South Pacific Current. *Journal of Physical Oceanography*, **25**, 77–91.

Tomczak, M., and J. Godfrey, 1994: *Regional Oceanography: An Introduction*. 1st ed., Pergamon Press.

Tsuchiya, M., 1981: The origin of the Pacific Equatorial 13° C Water. *Journal of Physical Oceanography*, **11**, 794–812.

Tsuchiya, M., and L. Talley, 1996: Water-property distributions along an eastern Pacific hydrographic section at 135° W. *Journal of Marine Research*, **54**, 541–564.

Tsuchiya, M., and L. Talley, 1998: A Pacific hydrographic section at 88° W: water-property distribution. *Journal of Geophysical Research*, **103**(C6), 12,899–12,918.

Wijffels, S., J. Toole, and R. Davis, 2001: Revisiting the South Pacific subtropical circulation: A synthesis of World Ocean Circulation Experiment along 32° S. *Journal of Geophysical Research*, **106**(C9), 19,481–19,513.

Wong, A., G. Johnson, and W. Owens, 2003: Delayed-mode calibration of autonomous CTD profiling float salinity data by θ-S climatology. *Journal of Atmospheric and Oceanic Technology*, **20**(2), 308–318.

Zhang, Y., J. Wallace, and D. Battisti, 1997: Enso-like interdecadal variability: 1900-93. *Journal of Climate*, **10**, 1004–1020.

Printed January 22, 2003.

Figure Captions

FIG. 1. Locations of vertical profile data used in this study: WOCE one-time CTD sections (dots, labeled P6, P15-P19, P21), Argo float tracks (thin solid lines, labeled 1-10), the Aug-Sep 1998 PX81 high resolution XBT track line (thick dashed line). Spatial extent of SPESTMW (thick solid line) as determined by the WOCE sections is also shown.

FIG. 2. Potential temperature (contoured at 1° C intervals) in the upper 350 dbar, between the equator and 40° S, along three meridional WOCE CTD sections. (a) P19 at 88° W. (b) P18 at 103° W. (c) P17 at 135° W. Shaded parts are regions below the mixed layer where $|Q|$ is less than 3×10^{-10} m^{-1} s^{-1}. See Fig. 1 for section locations.

FIG. 3. Following Fig. 2, but displaying salinity (contoured at 0.2 PSS-78 intervals).

FIG. 4. Following Fig. 2, but displaying potential density (contoured at 0.2 kg m^{-3} intervals).

FIG. 5. θ-S plot of SPESTMW ($|Q| < 3 \times 10^{-10}$ m^{-1} s^{-1}, $25.0 < \sigma_\theta < 25.7$ kg m^{-3}) along WOCE sections P19, P18 and P17. Lines of constant σ_θ are superimposed.

FIG. 6. Time series of (a) pressure (dbar) of the mixed layer base, here taken as where $|Q| \approx 3 \times 10^{-10}$ m^{-1} s^{-1}, (b) potential density (kg m^{-3}) at 20 dbar, (c) potential temperature (° C) at 20 dbar, and (d) corrected salinity (PSS-78) at 20 dbar, of float 10 (WMO ID 59019). Time series go from July 2000 to January 2003.

FIG. 7. Time series of (a) potential temperature (contoured at 1° C intervals), (b) corrected salinity (contoured at 0.2 PSS-78 intervals), and (c) potential vorticity (contoured at 0.5×10^{-10} m^{-1} s^{-1} intervals), in the upper 300 dbar, of float 10 (WMO ID 59019). The two bounding isopycnals of SPESTMW, 25.0 and 25.7 kg m^{-3}, are overlain in white.

FIG. 8. Following Fig. 7, but of float 5 (WMO ID 59016).

FIG. 9. (a) Potential temperature (contoured at 1° C intervals), (b) estimated salinity (contoured at 0.2 PSS-78 intervals), and (c) estimated potential density (contoured at 0.2 kg m^{-3} intervals), in the upper 300 dbar, from the equator to 35° S, along PX81 XBT line sampled during Aug-Sep 1998. Shaded regions denote areas below 30 dbar with estimated $|Q|$ less than 3×10^{-10} m^{-1} s^{-1}. See Fig. 1 for the Aug-Sep 1998 PX81 line location.

FIG. 10. Map of South Pacific subduction rates from Huang and Qiu (1998) (shaded contours of 0, 20, 40, 80, and 160 m $year^{-1}$) with 25.0 and 25.7 kg m^{-3} maximum surface isopycnals (thick solid lines) from the monthly World Ocean Atlas 1998 climatology (Antonov et al. (1998), Boyer et al. (1998)). Spatial extent of SPESTMW (thick dashed line) as determined by the WOCE sections is also shown (as in Fig. 1).

FIG. 11. Stability ratio R_ρ (contoured between 2 and 1 with lower values shaded increasingly dark at 0.2 intervals) in the upper 350 dbar, between the equator and 40° S, along three meridional WOCE CTD sections. (a) P19 at 88° W. (b) P18 at 103° W. (c) P17 at 135° W. The two bounding isopycnals of SPESTMW, 25.0 and 25.7 kg m^{-3}, are contoured (thick lines).

FIG. 12. Stability ratio R_ρ along $\sigma_\theta = 25.5$ kg m^{-3}, for floats 9 (WMO ID 39031, solid line) and 10 (WMO ID 59019, dashed line). Time series go from July 2000 to January 2003.

Figure 1

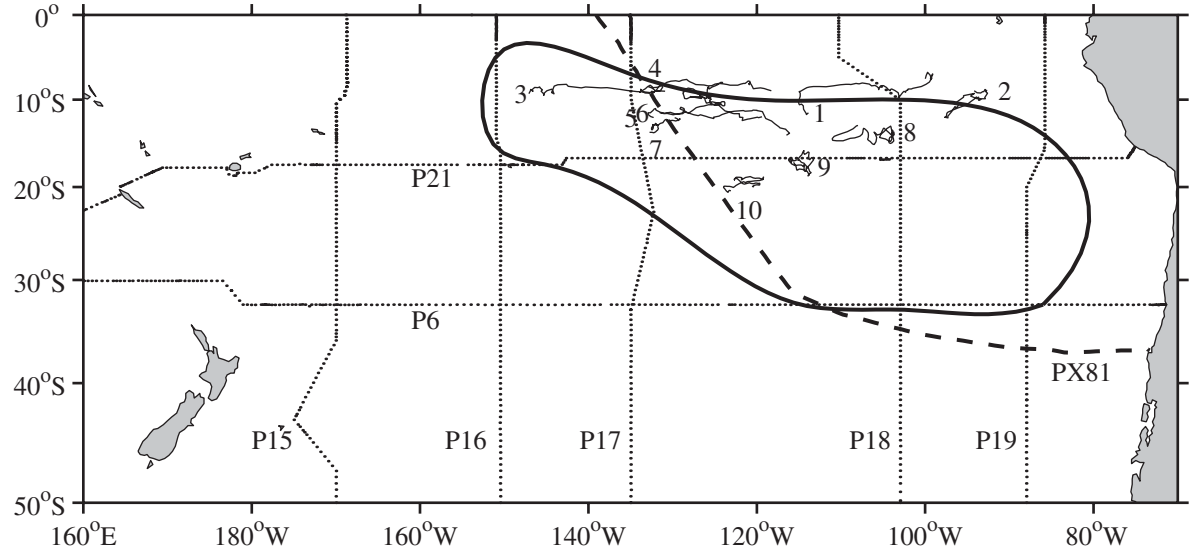
0°
10°S
20°S
30°S
40°S
50°S
160°E
180°W
160°W
140°W
120°W
100°W
80°W
1
2
3
4
5
6
7
8
9
10
P21
P6
P15
P16
P17
P18
P19
PX81

Figure 2

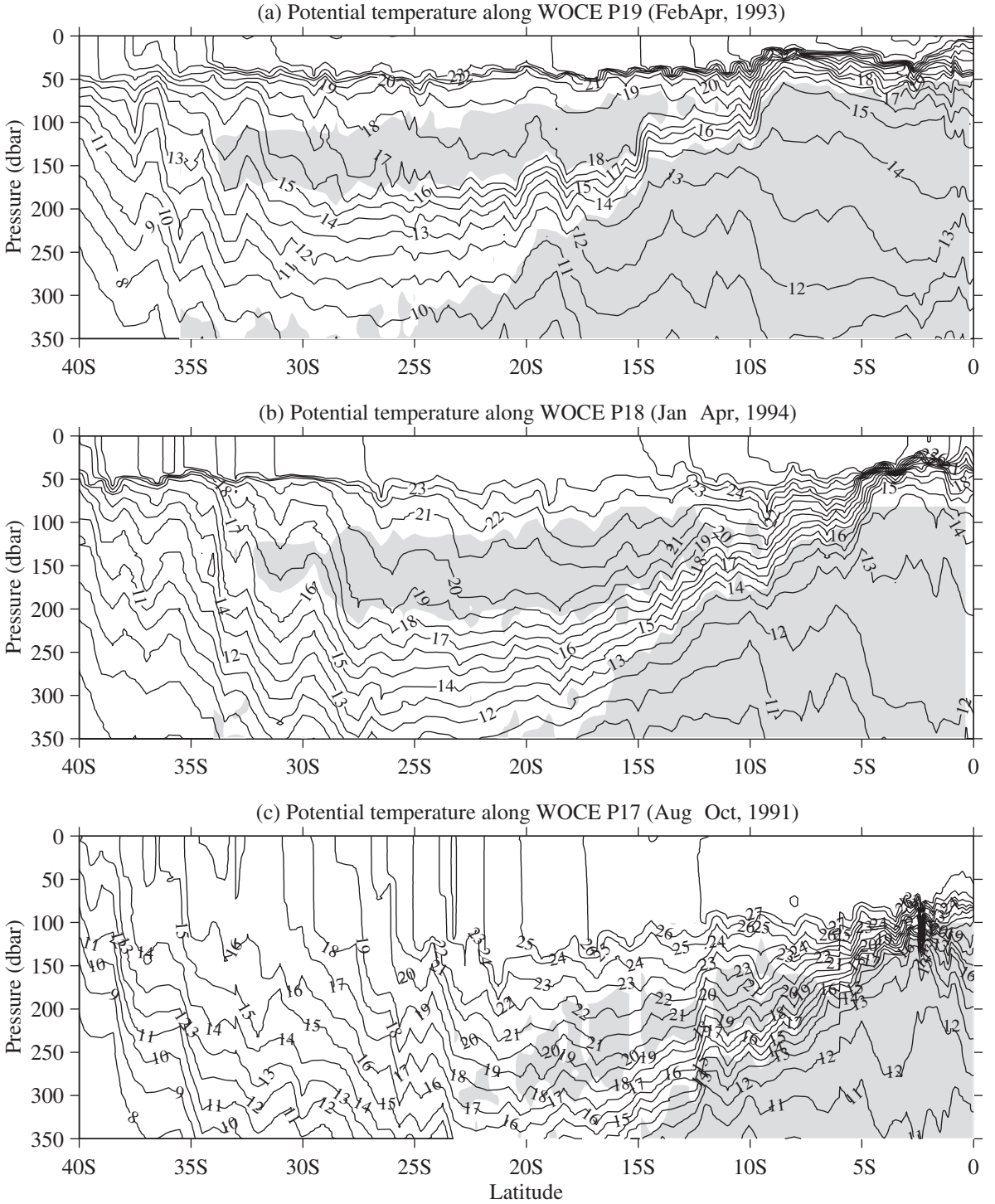
(a) Potential temperature along WOCE P19 (FebApr, 1993)
(b) Potential temperature along WOCE P18 (Jan Apr, 1994)
(c) Potential temperature along WOCE P17 (Aug Oct, 1991)
Pressure (dbar)
0
50
100
150
200
250
300
350
40S
35S
30S
25S
20S
15S
10S
5S
0
Latitude

Figure 3

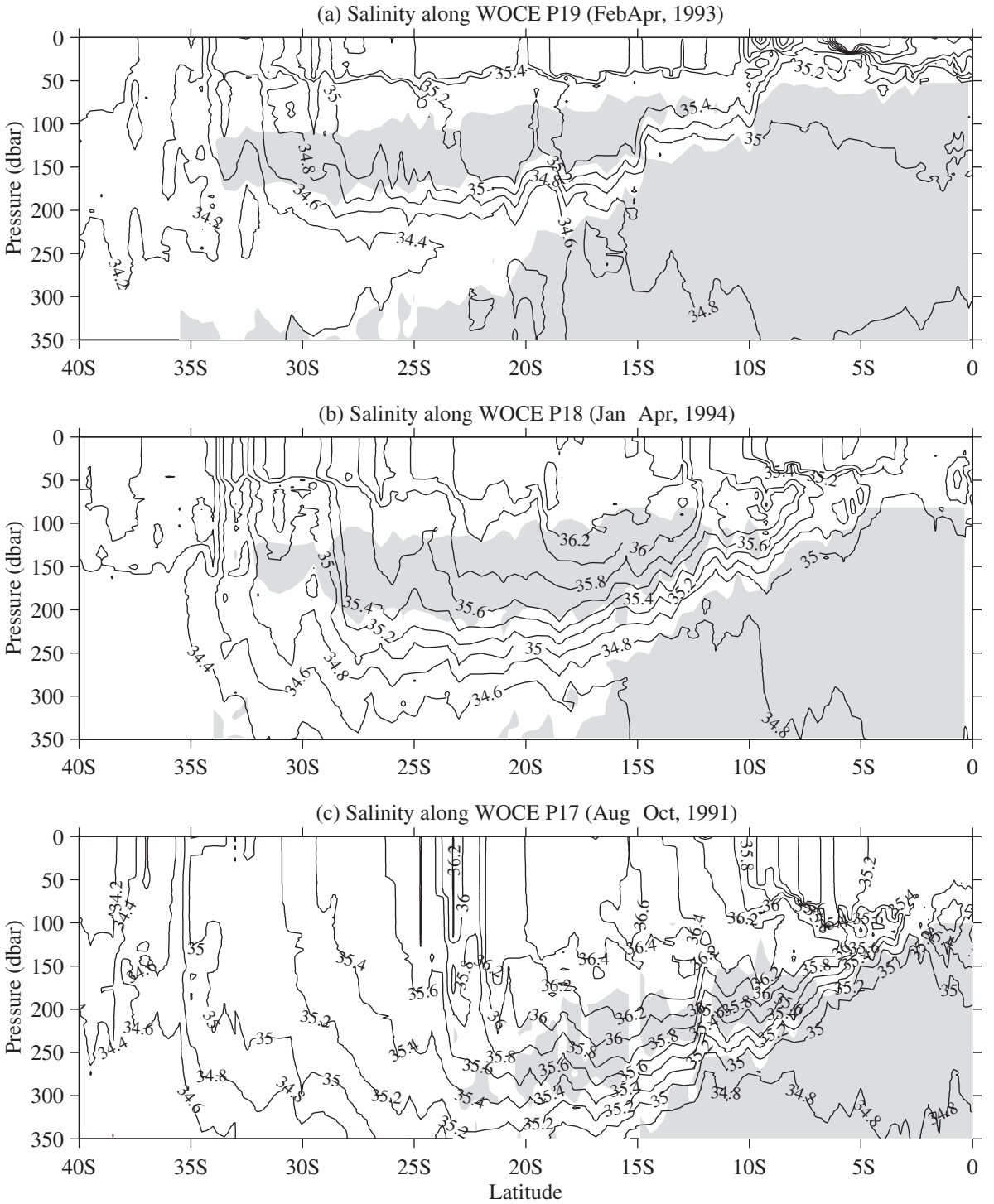
(a) Salinity along WOCE P19 (FebApr, 1993)
(b) Salinity along WOCE P18 (Jan Apr, 1994)
(c) Salinity along WOCE P17 (Aug Oct, 1991)
Pressure (dbar)
0
50
100
150
200
250
300
350
40S
35S
30S
25S
20S
15S
10S
5S
0
Latitude

Figure 4

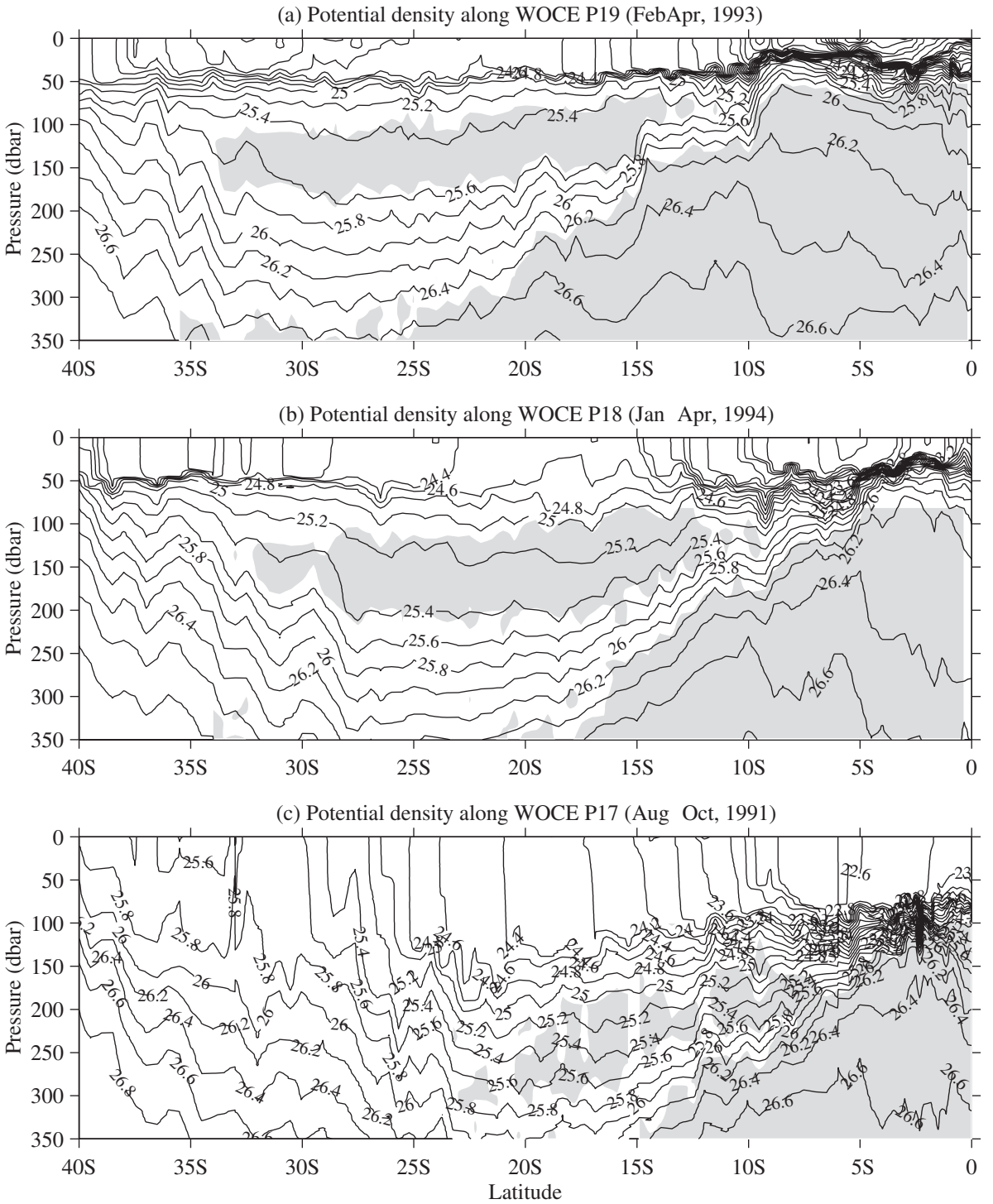
(a) Potential density along WOCE P19 (FebApr, 1993)
(b) Potential density along WOCE P18 (Jan Apr, 1994)
(c) Potential density along WOCE P17 (Aug Oct, 1991)
Pressure (dbar)
0
50
100
150
200
250
300
350
40S
35S
30S
25S
20S
15S
10S
5S
0
Latitude

Figure 5

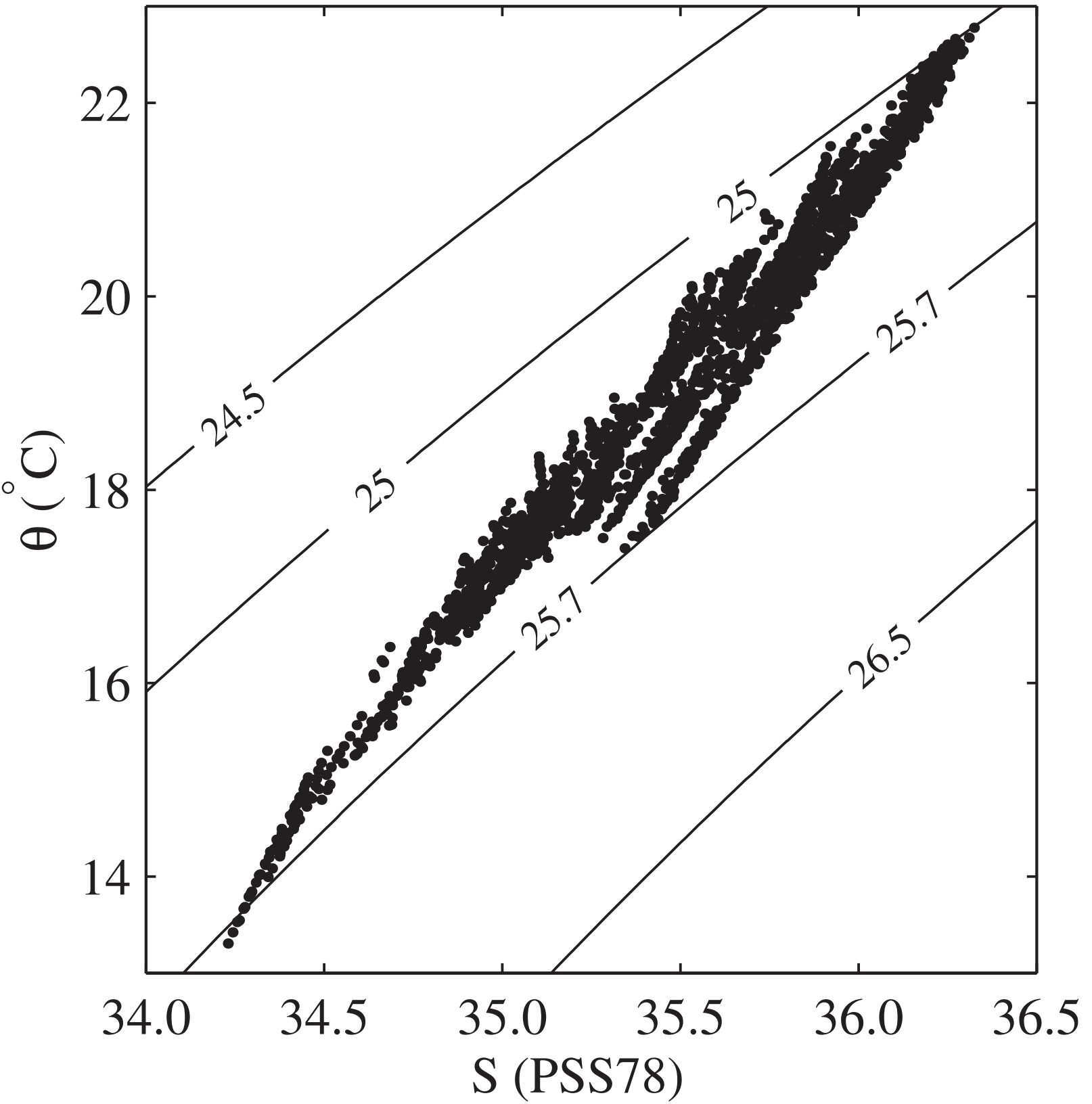
22
20
18
16
14
θ (°C)
24.5
25
25
25.7
25.7
26.5
34.0
34.5
35.0
35.5
36.0
36.5
S (PSS78)

Figure 6

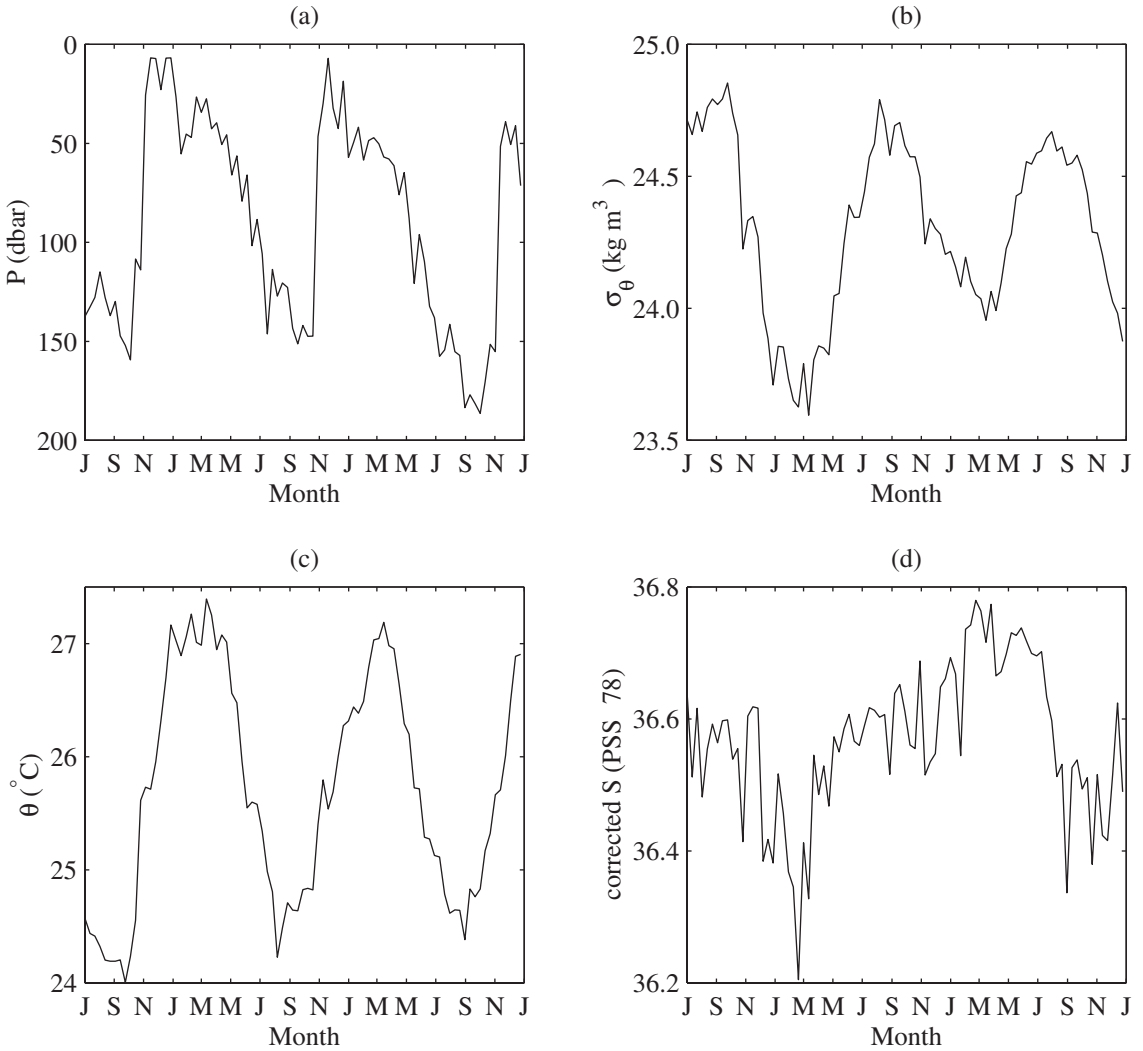
(a)
P (dbar)
0
50
100
150
200
J S N J M M J S N J M M J S N J
Month
(b)
σ_θ (kg m^3)
25.0
24.5
24.0
23.5
J S N J M M J S N J M M J S N J
Month
(c)
θ (°C)
27
26
25
24
J S N J M M J S N J M M J S N J
Month
(d)
corrected S (PSS 78)
36.8
36.6
36.4
36.2
J S N J M M J S N J M M J S N J
Month

Figure 7

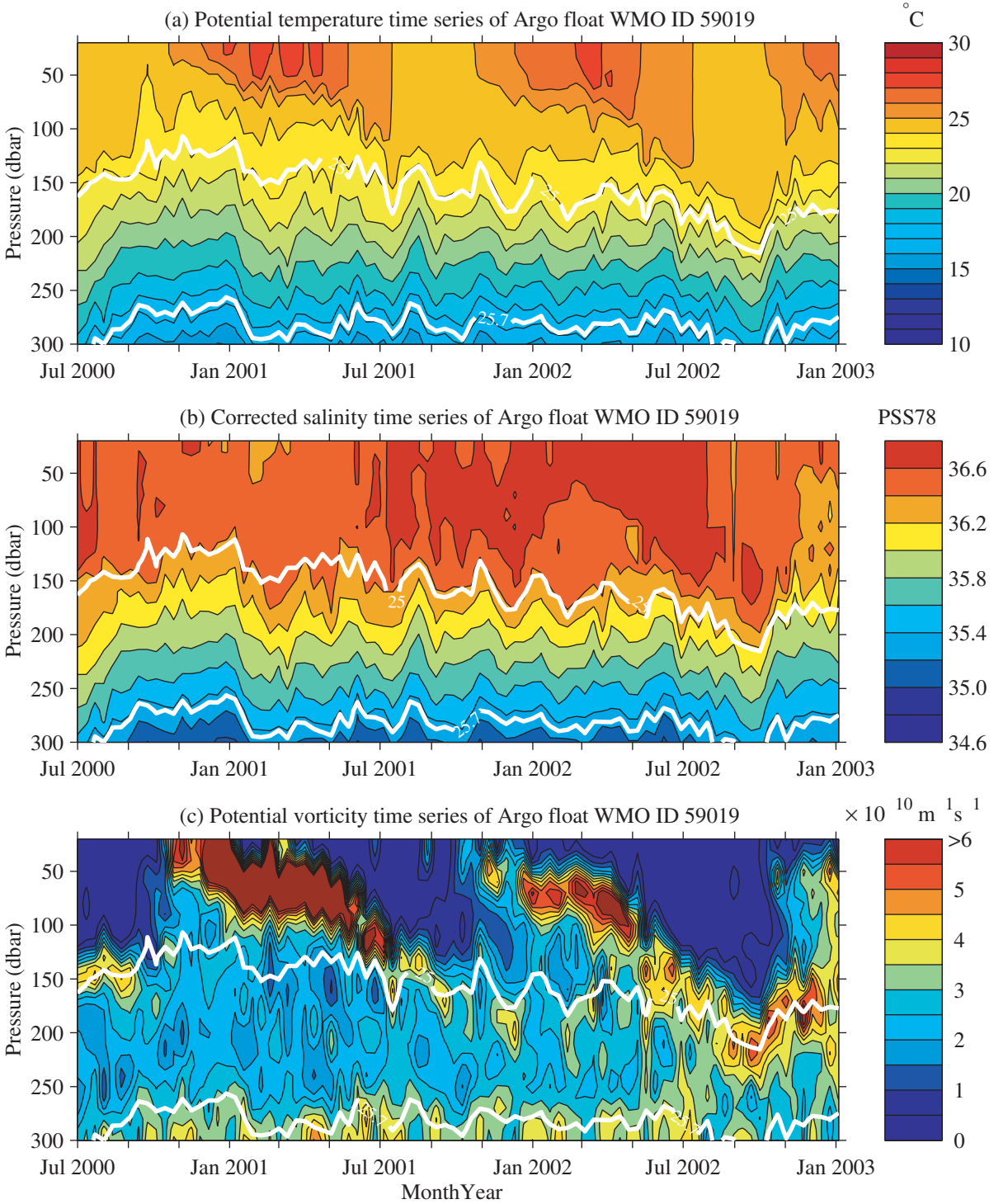
(a) Potential temperature time series of Argo float WMO ID 59019
°C
30
25
20
15
10
Pressure (dbar)
50
100
150
200
250
300
25.7
Jul 2000
Jan 2001
Jul 2001
Jan 2002
Jul 2002
Jan 2003
(b) Corrected salinity time series of Argo float WMO ID 59019
PSS78
36.6
36.2
35.8
35.4
35.0
34.6
25
25.7
(c) Potential vorticity time series of Argo float WMO ID 59019
× 10 10 m 1 s 1
>6
5
4
3
2
1
0
MonthYear

Figure 8

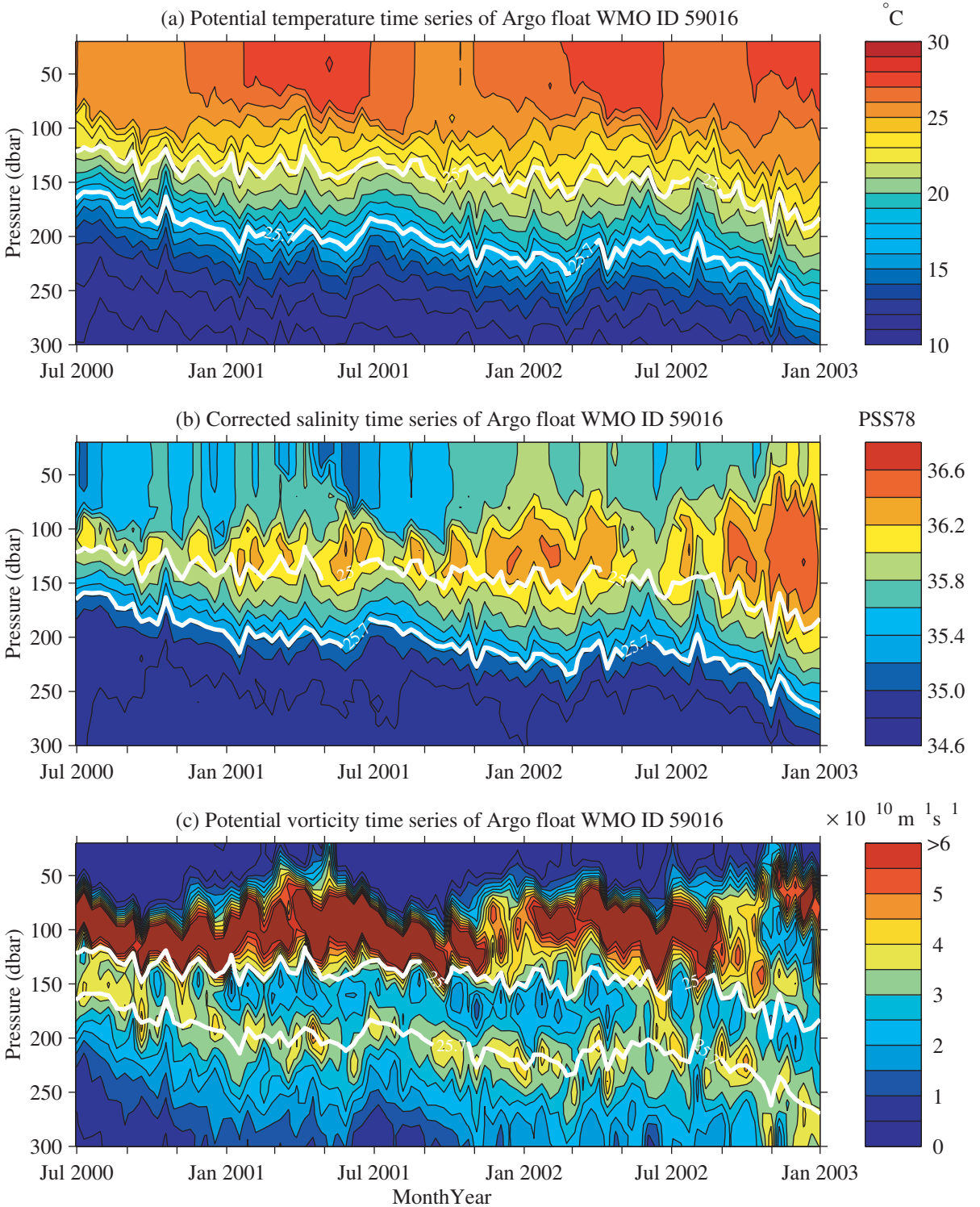
(a) Potential temperature time series of Argo float WMO ID 59016
°C
30
25
20
15
10
Pressure (dbar)
50
100
150
200
250
300
25.7
Jul 2000
Jan 2001
Jul 2001
Jan 2002
Jul 2002
Jan 2003
(b) Corrected salinity time series of Argo float WMO ID 59016
PSS78
36.6
36.2
35.8
35.4
35.0
34.6
(c) Potential vorticity time series of Argo float WMO ID 59016
× 10 10 m 1 s 1
>6
5
4
3
2
1
0
MonthYear

Figure 9

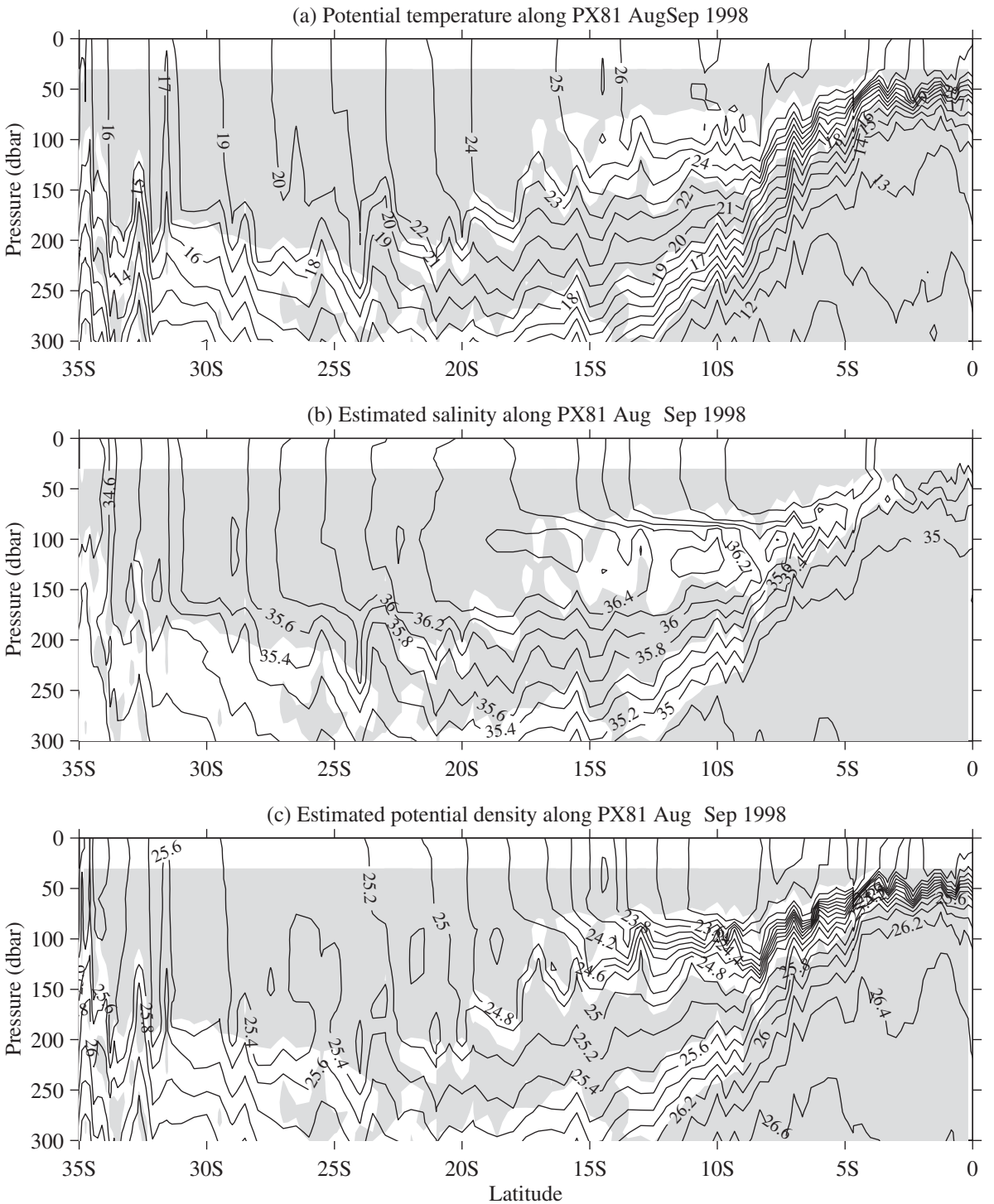
(a) Potential temperature along PX81 AugSep 1998
Pressure (dbar)
0
50
100
150
200
250
300
35S
30S
25S
20S
15S
10S
5S
0
(b) Estimated salinity along PX81 Aug Sep 1998
Pressure (dbar)
(c) Estimated potential density along PX81 Aug Sep 1998
Pressure (dbar)
Latitude

Figure 10

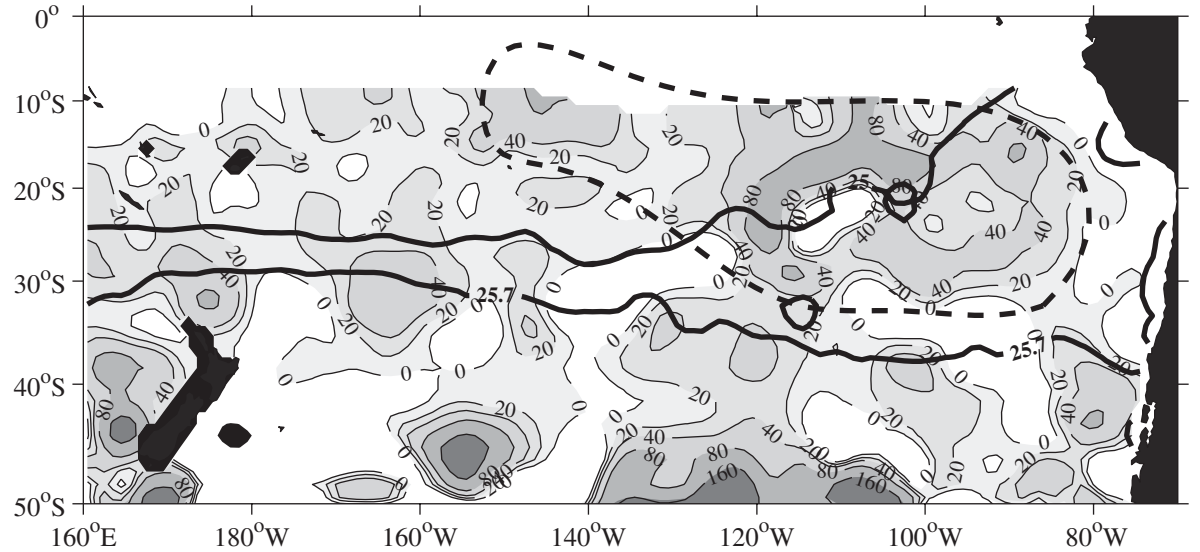

Figure 11

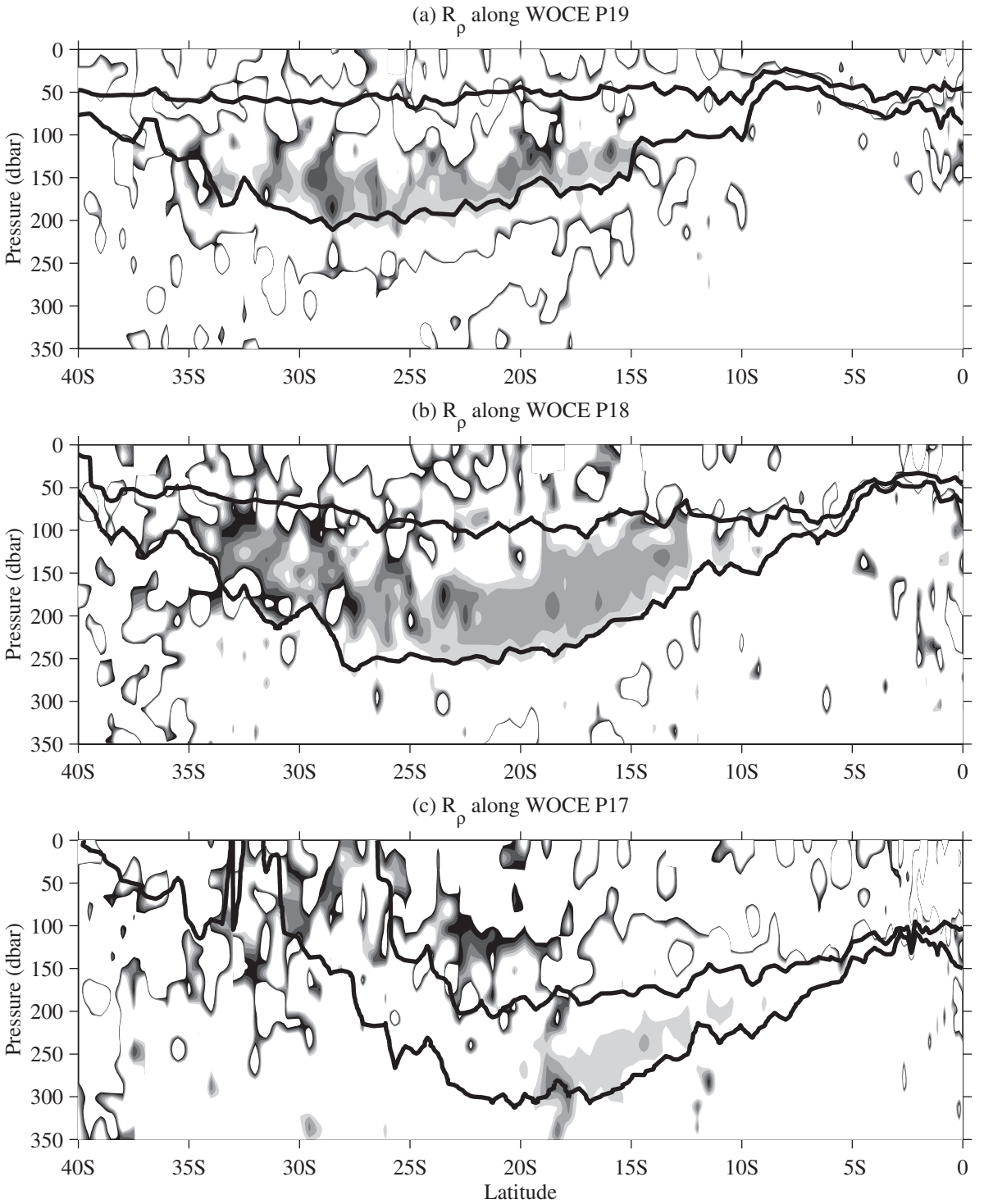
(a) R_ρ along WOCE P19
(b) R_ρ along WOCE P18
(c) R_ρ along WOCE P17
Pressure (dbar)
0
50
100
150
200
250
300
350
40S
35S
30S
25S
20S
15S
10S
5S
0
Latitude

Figure 12

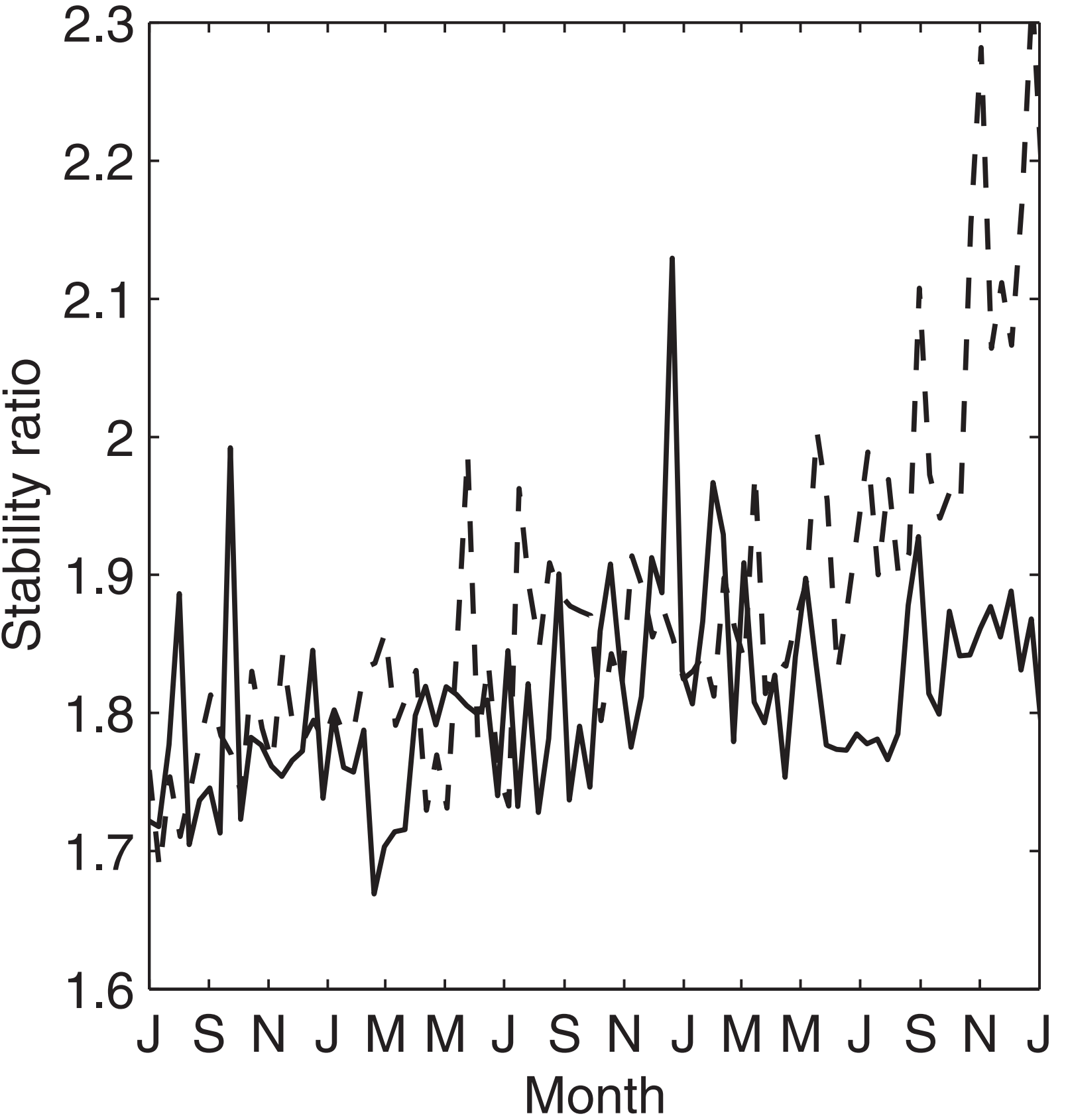
2.3
2.2
2.1
2
1.9
1.8
1.7
1.6
Stability ratio
J S N J M M J S N J M M J S N J
Month